JOURNAL OF GEOPHYSICAL RESEARCH, VOL. 105, NO. A12, PAGES 27,119–27,130, DECEMBER 1, 2000

Mesospheric gravity wave imaging at a subauroral site: First results from Millstone Hill

Steven M. Smith, Michael Mendillo, and Jeffrey Baumgardner

Center for Space Physics, Boston University, Boston, Massachusetts

Ronald R. Clark

Department of Electrical and Computer Engineering, University of New Hampshire, Durham

Abstract. Optical detections of short-period quasi-monochromatic gravity waves in the mesospheric nightglow emissions of OH (695–950 nm), O (557.7 nm), and Na (589.3 nm) have been obtained for the first time from Millstone Hill, Massachusetts (42.6°N, 71.5°W). Using a new all-sky bare charge-coupled device (CCD) imaging system at this subauroral site, we obtained 12 nights of observations during the period February 1 to July 21, 1998. Wave structure was observed during ~55% of the total observing time, and 35 events were identified and analyzed. Two types of wave structure were observed: extensive, long-lasting (~1–5 hours) waves known as bands and small-scale, short-lived (~5–40 min) features called ripples. The band events are believed to be due to freely propagating or ducted internal gravity waves. The mean measured parameter values of the band events were horizontal wavelength (λ_h) = 21±7 km, phase speed (c_{ob}) = 47±20 m s^{-1}, and observed period (τ_{ob}) = 8.5±4.6 min. The intrinsic wave parameters (c_{in} and τ_{in}) and the vertical wavelength (λ_z) of the band events were calculated using available meteor radar winds for nine of the events. Of the deduced λ_z values, five were evanescent, and the remaining four ranged from 12 to 21 km, with a mean of 17±4 km. Calculated energy and momentum fluxes for two case study events yielded 4–14×10^{-3} W m^{-2} and 5–30 m^2 s^{-2}, respectively. Possible sources of the waves were investigated using additional data obtained during 1999. The majority of the events exhibited poleward propagation, even during periods of visible auroral activity. This indicates that although the thermosphere above Millstone Hill exhibits subauroral behavior during enhanced levels of geomagnetic activity (Kp>3), the propagation characteristics and frequency of occurrence of mesospheric gravity waves at this location differ very little from other middle- and low-latitude locations.

1. Introduction

Short-period (τ<1 hour) internal gravity waves (IGWs) at upper mesospheric heights (80–100 km) are known to contribute significantly to global wind circulation [*Hines*, 1972; *Fritts*, 1984; *Garcia and Solomon*, 1985; *McLandress*, 1998] and to the energy and momentum budgets by their interaction with the mean wind field in this region [*Booker and Bretherton*, 1967; *Taylor et al.*, 1993]. The occurrence of mesospheric gravity waves is irregular, so it is important that in order to better understand the dynamics of this region the spatial and temporal morphology of mesospheric gravity waves are quantified.

Paper number 1999JA000343.
0148-0227/00/1999JA000343$09.00

To advance this goal and in preparation for the NASA Thermosphere-Ionosphere-Mesosphere Energetics and Dynamics (TIMED) mission of joint ground-based/space-based studies, a multidiagnostic program of optical radar research on mesospheric gravity waves above Millstone Hill is being developed. This program will involve collaborative studies using an imaging Fabry-Perot interferometer (FPI) [*Biondi et al.*, 1995], a Rayleigh scattering lidar [*Sipler et al.*, 1999], and the CEDAR (Coupling, Energetics, and Dynamics of Atmospheric Regions) all-sky imaging facility [*Baumgardner et al.*, 1993], all sited at Millstone Hill. These instruments will provide two-dimensional context images, horizontal winds, wave structures, and possible temperature information. In particular, the FPI will obtain horizontal neutral winds from mesospheric OH and OI emission measurements, enabling intrinsic wave parameters to be deduced. The lidar will measure the atmospheric temperature and density up to at least 85 km.

Table 1. Emission Layer Characteristics and Observational Parameters Used in This Study

Emission Layer	Layer Height, km	Layer Thickness, km	Filter Wavelength, nm	Filter Bandwidth, nm	Integration Time, s	Height and Thickness References
OH	87	6–10	695~950	235	30	*Baker and Stair* [1988]
Na (doublet)	90	8–10	589.3	1.4	120	*Greer and Best* [1967] *Newman* [1988]
OI(^{1}S)	96	8–12	557.7	1.2	120	*Thomas and Young* [1980] *Ward et al.* [1995]
Background	–	–	644.4	1.2	120	–
Cloud	–	–	760.0	10.0	30	–

In addition, data obtained from the Boston University CEDAR Optical Tomographic Imaging Facility (COTIF) chain of spectrographs [*Semeter and Mendillo*, 1997; *Semeter et al.*, 1999] will allow optical tomographic reconstruction of some of the IGW events in height and latitude. This study utilized a new CCD camera that was undergoing a field test checkout in preparation for its use in nonaeronomic studies at another site. The regular CEDAR imager at Millstone Hill is an image-intensified CCD that, while capable for *F* region/thermospheric studies, does not record mesospheric emissions unless unusually bright.

Gravity wave imaging was done initially with wide-field photography [*Peterson and Kieffaber*, 1973, 1975; *Moreels and Herse*, 1977; *Peterson*, 1979; *Armstrong*, 1982; *Clairemidi et al.*, 1985] and subsequently with all-sky imagers [*Taylor et al.*, 1987, 1991, 1995a, b, c, d, 1997; *Taylor and Hapgood*, 1988; *Hecht et al.*, 1994; *Swenson et al.*, 1995; *Gardner et al.*, 1996; *Isler et al.*, 1997]. All-sky imaging provides a unique and unambiguous record of the occurrence and propagation directions of mesospheric gravity waves. The images result from the integration of the gravity wave field over the emission layer thickness (~8–10 km, see Table 1). As a result, imagers are only sensitive to waves with vertical scale sizes greater than this.

Two different types of quasi-monochromatic wave structure are observed in all-sky images, and both are manifest as subtle, wave-like intensity variations (~1–5%) in the background emission. Band events [*Taylor and Hapgood*, 1990; *Taylor et al.*, 1995a, b, c] are the most common type. They typically exhibit horizontal wavelengths >15 km and have wave fronts that usually cover the entire sky. These events are usually long-lived, typically lasting several hours. Band events are believed to be due to IGWs that propagate freely, horizontally and vertically, or that have been ducted by vertical wind or temperature shears in the mesosphere [*Isler et al.*, 1997; *Walterscheid et al.*, 1999]. Ripple events [*Peterson*, 1979; *Taylor and Hapgood*, 1990; *Taylor and Hill*, 1991; *Taylor et al.*, 1995a, b, c, 1997], appear to be another type of wave activity and are characterized by relatively short lifetimes (<45 min) and small spatial extent (~10^3 km^2). They typically exhibit horizontal wavelengths of <10 km and oscillation periods near the Brunt-Vaisala period (4–6 min) [*Taylor et al.*, 1997]. In this initial study we will concentrate on the characteristics of the band events as these are more important in the context of IGW energy and momentum transport into the mesosphere and lower thermosphere (MALT) region. A study of the ripple events will be left for a future study.

The sources of gravity waves are not known with certainty. Energetic processes in the auroral zone have been identified as a source in high-latitude studies [*Francis*, 1975; *Hunsucker*, 1982; *Clairemidi et al.*, 1985]. At midlatitudes, orographic forcing, jet streams, and tro-

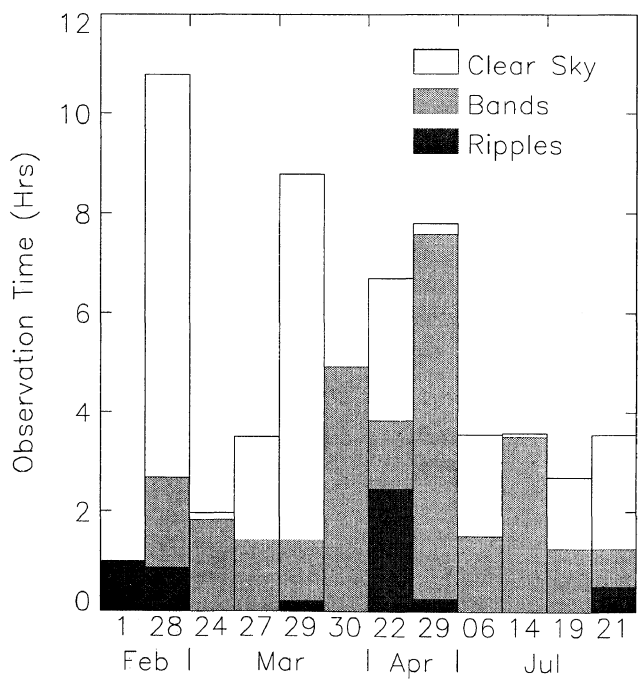

Figure 1. Frequency of occurrence of the mesospheric wave-like structures observed at Millstone Hill during the 1998 imaging campaign.

pospheric storm fronts have been suggested as sources [*Freund and Jacka*, 1979; *Krassovsky et al.*, 1977; *Garilov and Shved*, 1982; *Taylor and Hapgood*, 1988; *Taylor et al.*, 1995d; *Swenson and Espy*, 1995; *Dewan et al.*, 1998]. Millstone Hill, Massachusetts (42.6°N, 71.5°W), is situated near the transition region between midlatitudes and the auroral zone. Its subauroral position, its proximity to the Atlantic Ocean, and its large distance from major mountain ranges make it an excellent site for the investigation of both auroral and meteorological sources in the generation of IGWs and their subsequent propagation in the mesosphere. Mesospheric gravity wave measurements from the northeastern region of the United States have not been reported previously.

2. The All-Sky Imaging System

The all-sky imaging system used in this study employed a back-illuminated, bare CCD consisting of 1024 x 1024 pixels, thermoelectrically cooled to -50C°. The CCD chip had a quantum efficiency of ~80–83% in the visible region of interest and ~86–38% in the 695- to 950-nm near-infrared (NIR) region. During normal operation the CCD had a dark current of ~1 el^- $pixel^{-1}$ s^{-1}. Each image was 2×2 binned and digitized to 16-bit resolution. The all-sky camera system employed a Sigma 15 mm f/2.8 fish-eye lens, providing a 180° field of view. Trees surround the Millstone site, so features could be discerned usefully at zenith distances down to ~70°. For wave features at 90 km this corresponds to a horizontal distance of ~460 km radially from Millstone Hill, or a total viewing area of ~6×10^5 km^2. The system can record $\Delta I/\overline{I}$ variations of less than 0.5–1%, where ΔI is the amplitude of the height-integrated volume emission brightness with respect to $\overline{I}$, the mean brightness of the undisturbed emission layer. The pixel resolution of the imaging system at 90 km at zenith corresponds to 0.3 km. The camera was fitted with a rotating filter wheel which housed six narrowband interference filters. Table 1 lists the various emission wavelengths imaged and the typical integration times employed. Two mesospheric species (OI, OH) were regularly observed, and the Na filter was added later in this pilot project. Two filters, 644.4 nm (background) and 760.0 nm, enabled monitoring of ambient scattered light and cloud cover conditions. The sixth filter position was occupied by a 630.0-nm filter used for thermospheric studies [*Mendillo et al.*, 1989]. During single-emission studies, images of the OH emission were obtained every 40 s (nominal integration time + readout time); OI and Na images were obtained every 130 s. During multi-emission observing modes, images at each emission wavelength were obtained sequentially about every 5 min.

3. Observed Wave Parameters

The imaging data used in this initial search for mesospheric IGWs were obtained on 12 clear, moonless nights between February 1 and July 21, 1998. A total of ~59 hours of clear-sky image data was obtained, and wave activity was observed in one or more of the emissions ~55% of the time. Figure 1 illustrates the frequency of occurrence of structured activity in the OH, OI, and Na emissions on the 12 nights. Thirty-five separate wave events were observed in one or more of the nightglow emissions; of these events, 20 were band-type IGWs (Table 2), and 15 were of the ripple type.

Figure 2 shows examples of the wave events seen at Millstone Hill. Figures 2a and 2b are raw images showing bands in the OI and OH emissions on March 30, 1998. Figures 2c and 2d are examples of time-difference images which were created by subtracting two successive images [*Swenson and Espy*, 1995], in these cases, of OH and Na emission. Time differencing greatly increases the contrast of the resulting image and illustrates the motion of a feature. The high S/N ratio of the images allowed analysis without the need for time differencing.

During analysis the spatial distortion inherent in the all-sky imaging system was removed using known star positions in the images. The images were then mapped onto a surface corresponding to the nominal heights of the layers (see Table 1). The horizontal wavelength (λ_h) and observed phase velocity (c_{ob}) of the waves were measured from such "unwarped" images. The observed period (τ_{ob}) values were calculated from these parameters and are listed in Table 2.

The typical uncertainties associated with the λ_h and c_{ob} values were 4 and 11%, respectively. The uncertainty in the horizontal direction of wave propagation was less than 5°. The occurrence times of each event (Table 2) are given in UT, where UT = LT + 5 hours.

The wave fronts of the band events were essentially linear with little or no curvature. This indicated that the waves originated either from an extended source, such as a frontal system or a jet stream, or from a discrete source, such as a thunderstorm cell that was situated a large distance (~1000 km or more) from the Millstone Hill site. Occasionally, the all-sky emission would appear similar to a choppy ocean surface. This was indicative of a superposition of several waves with random propagation directions.

Figure 3 shows various observed parameters associated with the band events. Figure 3a is a polar plot of the observed horizontal phase velocities; Millstone Hill is at the center, and the length and direction of each vector represent the propagation speed and direction of each event. The direction azimuth is measured clockwise from north. The bands clearly exhibited a tendency for northward and eastward propagation, with all but two of the vectors in the 45°±90° azimuth range. During 11 of the band events, ripples were also seen; the differences between the simultaneous band/ripple propagation directions typically ranged from 10° to 80°.

Figures 3b and 3c give histograms of the measured c_{ob} and λ_h parameters. The c_{ob} values were typically

Table 2. Wave Parameters of the Band Events Recorded at Millstone Hill, February 1 to July 21, 1998

Date	Layer	Time, UT	λ_h, km	c_{ob}, m s^{-1}	Azimuth, °N	τ_{ob}, min	u, m s^{-1}	λ_z, km
Feb. 1	OH	0225–0325	29.6	36	325	13.7	–	–
Feb. 28	OI	0100–0340	36.8	39	100	15.8	–	–
March 24	OH	0310–0500	20.6	86	5	4.0	–	–
March 27	OI	0715–0840	13.1	28	333	7.7	-6	16
Mar 29	OH	0155–0220	11.3	74	209	2.5	–	–
	OI	0630–0730	32.3	55	85	9.8	–	–
March 30	OH	0450–0945	21.4	43	121	8.2	0	19
	OI	0450–0945	22.7	44	121	8.7	-9	21
April 22	OH	0930–0950	11.6	44	338	4.4	-5	∞
	OI	0600–0950	13.9	45	338	5.1	-30	∞
	OH	0600–0950	22.8	54	20	7.1	19	12
	OI	0635–0950	18.4	89	20	3.5	-47	∞
April 29	OH	0215–0445	17.4	81	55	3.6	-65	∞
	OH	0425–0945	17.0	35	35	8.2	–	–
	OI	0705–0925	21.3	32	35	11.0	–	–
	OI	0320–0950	15.3	37	30	6.9	-45	∞
July 6	Na	0615–0745	16.4	34	155	8.2	–	–
Jul 14	OI	0200–0530	22.7	41	5	9.3	–	–
July 19	Na	0730–0845	21.4	29	20	12.2	–	–
July 21	Na	0330–0445	24.3	19	15	20.9	–	–

The dashes denote events in which meteor radar wind measurements were not available.

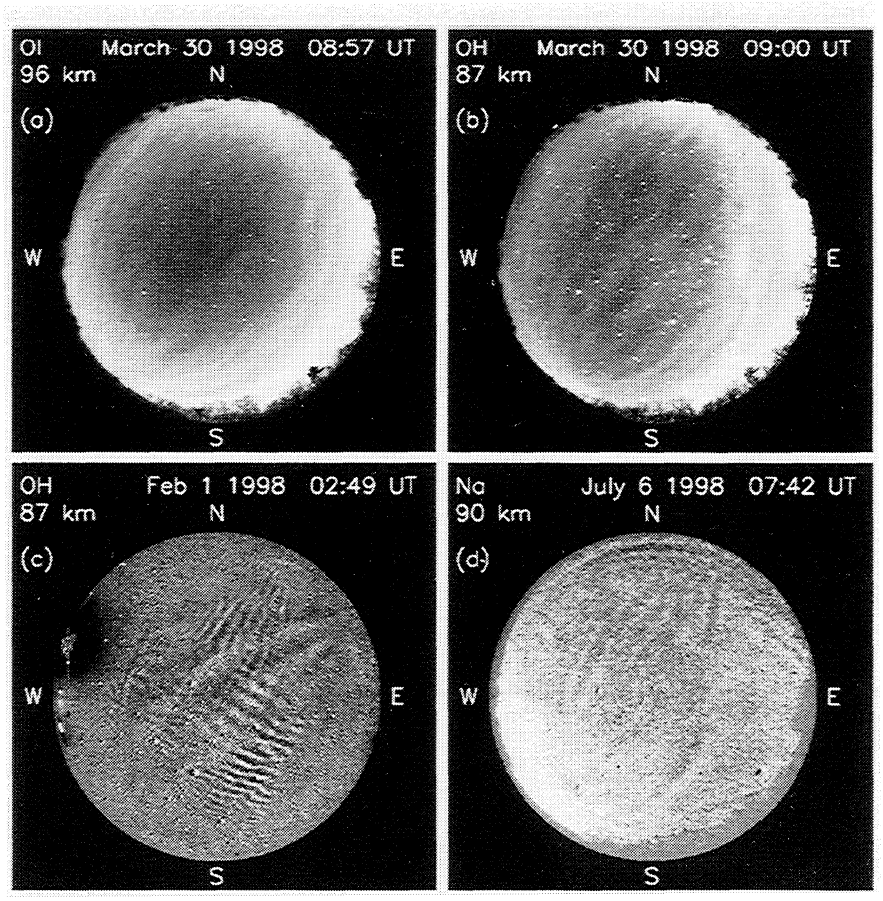

Figure 2. Emission images on March 30, 1998, showing extensive band structure for (a) raw OI and (b) raw OH. Time-difference image (see text) in OH emission taken on February 1, 1998, showing two ripple events together with a band event. (d) Time-difference image showing a band event in Na emission. This image has also been median-smoothed.

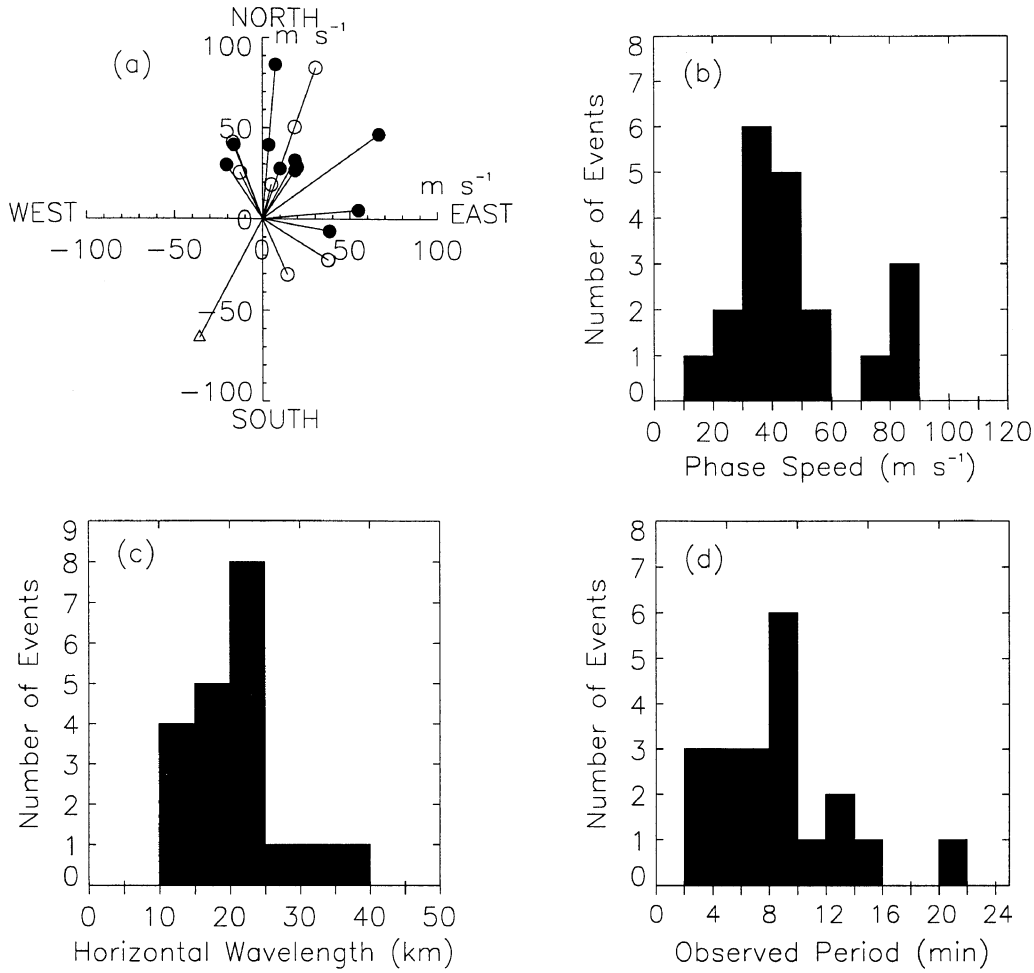

Figure 3. Characteristics of the 1998 band events observed at Millstone Hill (from Table 2). (a) Velocity vectors portrayed as lines extending from the origin to the circles. The symbols refer to the level of geomagnetic activity; solid circles (Kp=0–2), open circles (Kp=3–4), and open triangles (Kp=5–6). (b–d) Histograms of the number of events for the observed horizontal phase speed, horizontal wavelength, and period, respectively.

between 25 and 50 m s^{-1}, with a mean of 47±20 m s^{-1} (the uncertainty is the standard deviation). The λ_h values ranged from 10 to 25 km, with a mean of 21±7 km. Finally, in Figure 3d, the deduced τ_{ob} values can be seen to exhibit a broad range from 2 to 16 min, with a mean of 8.5±4.6 min. These values are typical of those reported in other studies, such as *Taylor's et al.*, [1995d, 1997].

4. Intrinsic Wave Parameters

The intrinsic wave parameters c_{in}, τ_{in}, and the vertical wavelength (λ_z) for each band event were deduced using available meteor radar wind measurements. Wind data were obtained from the University of New Hampshire (UNH) Meteor Radar System at Durham (43°N, 71°W) [*Clark*, 1978, 1983; *Clark and Salah*, 1991]. This system is a coherent pulsed radar operating at 36.8 MHz. The antenna system is a dual-beam system at 45° elevation with one beam directed to the northeast and one directed to the northwest. Phase-sequenced interferometers are used to determine the directions to the meteor trail targets yielding resolutions of 1° (rms) in both elevation and azimuth. This directional capability coupled with a range resolution of ±1 km yields a spatial resolution of the order of ±1 km for each raw wind measurement.

Radar wind data were available for nine events during the period March 27 to April 29, 1998. Hourly radar wind averages, centered at the nominal heights of the emission layers ±5 km, were used to derive the intrinsic wave parameters. Figure 4a is a histogram of the deduced τ_{in} values for the nine band events. The periods range from 2 to 11 min, with a mean of 5.2±3.1 min. The mean τ_{ob} value of these events was 6.1±2.0 min (Figure 3d), implying that the observed waves were, on average, Doppler-shifted to larger values by a factor of 17%. The values of u ranged from -65 to 20 m s^{-1} (Table 2), with a mean value of -21±27 m s^{-1}. The wind sign convention was positive in the direction of wave

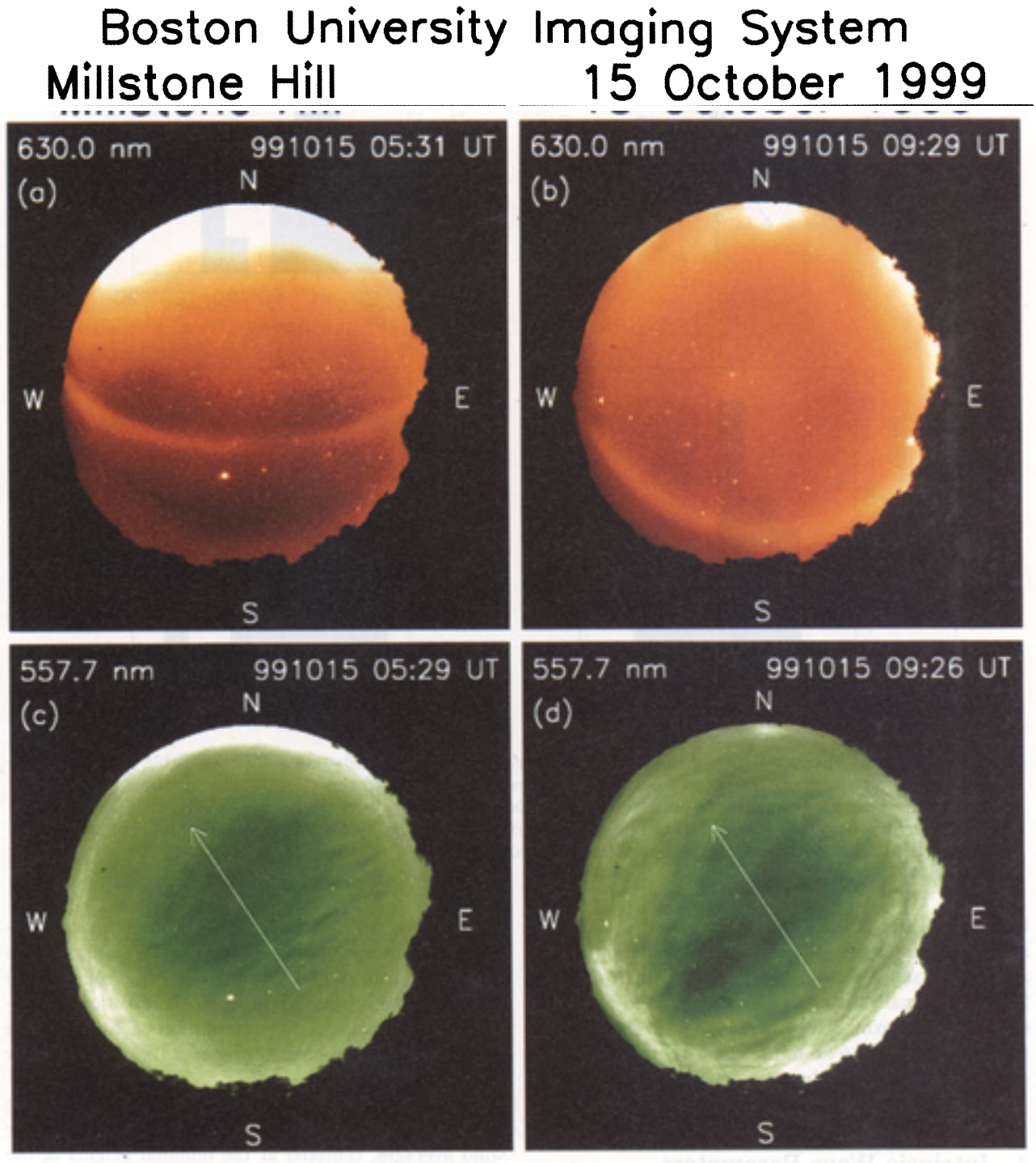

Plate 1. (a,b) Two 630.0-nm images showing diffuse aurora (h~200 km) to the north and a stable auroral red (SAR) arc (h~400 km) extending across the sky from east to west. This feature moved southward as the night progressed. (c,d) Two 557.7-nm images (h~96 km) from similar times showing mesospheric gravity waves propagating toward the northwest (arrows). The bright auroral images are not saturated but are the result of highlighting the fainter SAR arc. A small amount of cirrus cloud was present after 0800 UT.

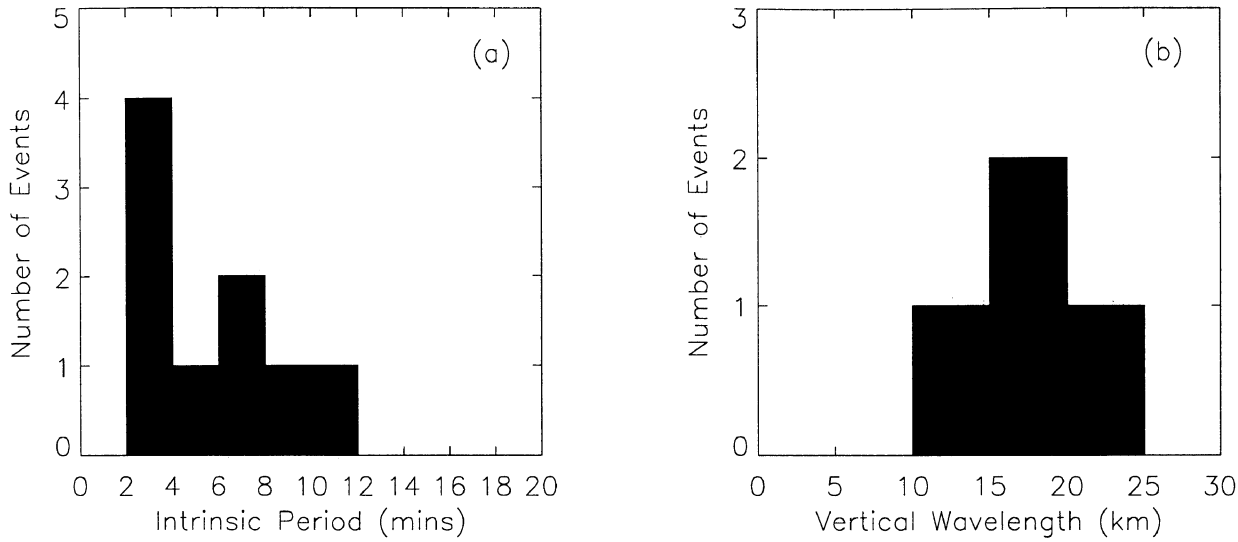

Figure 4. Histograms of the nine band events observed at Millstone Hill in 1998 for which there were radar wind measurements: (a) intrinsic periods and (b) vertical wavelengths.

propagation and negative in the opposite direction. All but one of the values were negative, indicating that the observed waves were generally propagating in the opposite direction to the mean wind flow.

Values for τ_b at the height of the emission layers were calculated using the following relation [*Taylor and Hapgood*, 1988]:

$$\tau_b = 2\pi[\frac{mg^2}{kT}\frac{(\gamma-1)}{\gamma} + \frac{g}{T}\frac{dT}{dz}]^{-1/2}, \quad (1)$$

where m is the mean molecular mass (4.84×10^{-26} kg), g is the acceleration due to gravity, z is the vertical distance, k is Boltzmann's constant, γ is the ratio of the specific heats, and T is the background temperature. Background temperature-height profiles were generated using the Mass Spectrometer Incoherent Scatter - Extension (MSIS-E) 1990 atmospheric model [*Hedin*, 1991]. Hourly averaged temperature values were calculated at the nominal height of the emission layer, and the temperature gradient was calculated over a vertical distance of 10 km centered on the layer. The calculated τ_b values ranged from 3.9 to 5.4 min, which is consistent with values found in the upper mesosphere.

5. Vertical Wavelengths

If one assumes an isothermal, horizontally stratified atmosphere, the vertical wavelength (λ_z) can be deduced using the approximated dispersion relation

$$m^2 = \frac{\omega_b^2}{(c_{ob}-u)^2} - l^2 - \frac{1}{4H^2}, \quad (2)$$

where ω_b is the Brunt-Vaisala frequency, H is the atmospheric scale height (~6 km), u is the magnitude of the mean wind in the direction of wave propagation, and m and l are the vertical and horizontal wavenumbers, respectively (where $m = 2\pi/\lambda_z$ and $l = 2\pi/\lambda_h$). Using (2), the λ_z values for the band events, derived from the available radar winds, are shown in Figure 4b. The λ_z uncertainty values ranged from ~50 to 100%, and resulted from uncertainties in the measured wave parameters and the radar wind values. Of the nine events, five (55%) were found to be evanescent, i.e., $\lambda_z = \infty$. The λ_z values for the four other events ranged from 12 to 21 km, with a mean of 17±4 km. The range of values is very similar to that found in the comprehensive studies by *Taylor et al.*, [1997] and *Isler et al.*, [1997].

The relatively large number of evanescent wave events found in this study is similar to that reported by *Isler et al.*, [1997] in which ~75% of the observed band events were either evanescent or ducted. This suggests that the majority of the quasi-monochromatic gravity waves observed with all-sky imagers are not freely propagating but are ducted. Evanescence occurs when vertical gradients in ω_b (due to temperature gradients) or in u cause $m^2<0$ in (2). A wave incident on an evanescent region will be partially or totally reflected and will also be strongly attenuated inside the region. Wave ducting can occur between two evanescent regions or between an evanescent region and the ground [*Isler et al.*, 1997], allowing the wave to travel many hundreds of kilometers with little or no attenuation. The temperature structure at 80–100 km, especially during the summer months, produces a ducting region, which is favorable for gravity waves of the scale sizes observed by all-sky imagers [*Walterscheid et al.*, 1999]. The amount of radar data available for this present study allowed only for the determination of hourly wind estimates at the height of each layer (±5 km) and did not yield suf-

ficiently well resolved vertical wind profiles, which are required in determining the presence of wind gradients that may be responsible for Doppler ducting of an incident wave.

6. Vertical Energy and Momentum Fluxes

Swenson and Liu [1998] used the analytical model of *Swenson and Gardner* [1998] to derive expressions for the vertical energy and momentum fluxes of an IGW propagating without loss in the OH emission at 87 km. The vertical energy flux (W m^{-2}) is

$$F_E = \frac{2.3 \times 10^{-3} \lambda_z^2}{CF^2 \lambda_h} \left(\frac{\Delta I}{\bar{I}}\right)^2. \quad (3)$$

The vertical momentum flux (m^2 s^{-2}) is

$$F_M = \frac{6 \times 10^4 \lambda_z}{CF^2 \lambda_h} \left(\frac{\Delta I}{\bar{I}}\right)^2, \quad (4)$$

where CF is the cancellation factor, which is the ratio of the intensity and neutral density perturbation ratios $((\Delta I/\bar{I})/(\Delta\rho/\bar{\rho}))$ and has the form

$$CF = 3.5\{1 - \exp[-0.0055(\lambda_z - 6)^2]\}. \quad (5)$$

The vertical energy and momentum fluxes associated with the two nonevanescent OH events on March 30 and April 22 (see Table 2) were calculated using these expressions. Both wave events exhibited intensity perturbation ratios $(\Delta I/\bar{I})$ of 2.1%. The March 30 event exhibited a vertical energy flux of 3.9×10^{-3} W m^{-2} and a vertical momentum flux of 5.4 m^2 s^{-2}. The April 22 event exhibited an energy flux of 14.3×10^{-3} W m^{-2} and a momentum flux of 30.3 m^2 s^{-2}. Both sets of values are consistent with values deduced from previous optical [*Wang et al.*, 1993; *Swenson and Liu*, 1998; *Swenson et al.*, 1999] and radar [*Vincent*, 1984; *Reid and Vincent*, 1987; *Meyer et al.*, 1989] studies. In particular, *Swenson et al.*, [1999] reported an average vertical energy flux of 12.8×10^{-3} W m^{-2} and an average vertical momentum flux of 21.9 ± 9.2 m^2 s^{-2} from OH imager measurements.

7. Possible IGW Sources

Several previous studies suggest that an important source of mesospheric IGWs is the strong convective activity associated with tropospheric storm fronts [*Freund and Jacka*, 1979; *Taylor and Hapgood*, 1988; *Taylor et al.*, 1995d; *Swenson and Espy*, 1995; *Dewan et al.*, 1998]. In particular, *Dewan et al.* [1998] presented the first direct evidence of gravity waves produced by thunderstorm activity.

An attempt to identify possible meteorological gravity wave source regions of the band events observed at Millstone Hill was made by using hourly radar summary maps of the continental United States obtained by the Next Generation Weather Radar system (NEXRAD) (National Climate Data Center (NCDC), NEXRAD National Mosaic Reflectivity Images, http://www4.ncdc.noaa.gov/cgi-win/wwcgi.dll?wwNexradImages2, 1998). The presence of strong convective activity was indicated by large echo strengths (>45 dB; 75 dB max). The meteorological information in the NEXRAD summary maps was confined to the continental United States, with only a small overlap around the border with Canada. Hence only events having propagation azimuths in the ranges 30° to 110° and 200° to 260° (~35% of the events) could be investigated, with very little information for other azimuths. As a result, no conclusive originating meteorological source or mechanism was found to be responsible for the IGW band events observed at Millstone Hill.

Another possible source is the sunrise/sunset terminator. At the latitude of Millstone Hill the terminator moves supersonically (~340 m s^{-1}) through the ozone layer, resulting in rapid heating/cooling at sunrise/sunset with the subsequent excitation of internal gravity waves. These waves would propagate westwards as a double shock front, ahead and behind the terminator [*Beer*, 1977], with a meridional component depending on the season. *Röttger* [1977] reported on evidence of F region gravity waves generated by this process. Such waves have been observed previously at Millstone Hill by *Galushko et al.* [1998] who reported incoherent scatter radar observations of IGWs in the 200- to 300-km height region. The waves were seen at sunrise propagating westward, perpendicular to the terminator, with a group velocity of 300–400 m s^{-1} and a period of 1.5–2 hours. Such waves would exhibit horizontal wavelengths of at least 100 km in the upper mesosphere. Because none of the observed wave events exhibited horizontal wavelengths of ~100 km or more, or speeds of ~300 m s^{-1}, we conclude that the sunrise/sunset terminator was not a source.

The Millstone Hill site is relatively far from large mountains to the west and close to the Atlantic Ocean to the east. Its subauroral location (53.0°N geomagnetic) means that one other possible IGW source is energetic processes in the auroral zone, such as particle precipitation and Joule heating, especially when auroral processes appear close to Millstone Hill [*Mendillo et al.*, 1989; *Foster et al.*, 1994].

The propagation directions of the majority of the wave events in 1998 (Figure 3a) tended to be northward and eastward, so an auroral source for the waves is unlikely. One event (March 29), however, did exhibit behavior that suggested an auroral origin. A set of OH bands propagated toward the southwest (azimuth = 209°) with c_{ob} = 74 m s^{-1}, which is much larger than the average velocity observed in this study. While Kp=5- during the event, it was not possible to rule out other sources, such as tropospheric sources to the north of Millstone Hill.

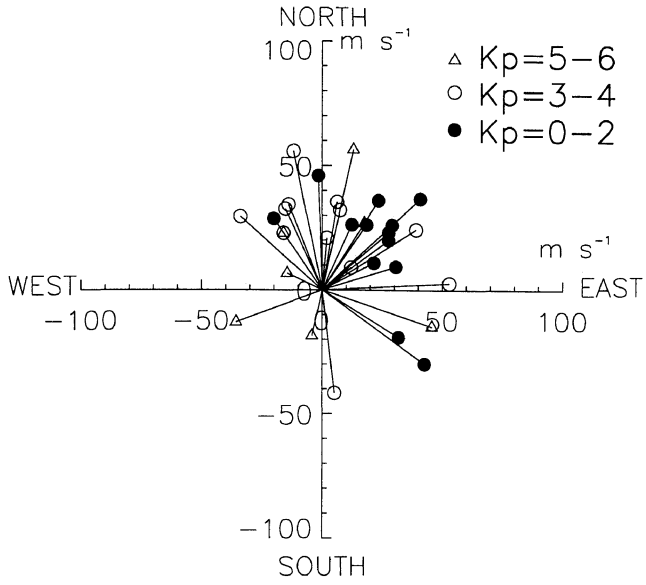

Figure 5. Velocity vectors, portrayed as lines extending from the origin to the circles, of the band events observed at Millstone Hill during the period May 12 to October 15, 1999. The symbols refer to the level of geomagnetic activity.

The number of events available for the 1998 pilot study was very limited during periods of enhanced levels of geomagnetic activity, i.e., $Kp>3$, so no conclusive result was found for the significance of auroral processes as a source of IGWs. However, this was investigated further by using additional 557.7-nm image data obtained on 21 nights during the period May 12 to October 15, 1999. These data yielded 31 band events. The horizontal wavelengths ranged from 8 to 80 km, with a mean of 23±12 km, and the velocities ranged from 20 to 57 m s^{-1}, with a mean of 37±12 m s^{-1}, values comparable to the 1998 events. There was also a tendency for the waves to propagate towards the north and east (see Figure 5) which is similar to the 1998 events (Figure 3a).

On 7 of the 21 nights the geomagnetic activity was moderate to high. This was indicated by either visible auroral activity in 557.7- and 630.0-nm all-sky images and/or $Kp>3$. The directions of the mesospheric wave events on these nights were investigated and are denoted in Figure 5 as open circles and triangles. The Kp values averaged 4+.

While 15 of the 31 events occurred on disturbed nights, only 3 exhibited southward components of motion. Two of these occurred on September 13, the night of highest magnetic activity (Kp=6) (azimuth=193° and 108° in Figure 5), and the other occurred on September 14 (azimuth=250°). Perhaps the most interesting waves occurred on the second most active night (October 15, Kp=5); all three wave events propagated toward the northwest. Plate 1 depicts 630.0- and 557.7-nm all-sky images taken 4 hours apart during this night. A bright auroral display can be seen clearly toward the north (Plates 1a and 1b) and the southward advance of

Table 3. A List of Several Previous Airglow Gravity Wave Imaging Studies of Band Events

Location	Geographic Latitude	Geomagnetic Latitude	c_{ob}, m s^{-1}	λ_h, km	τ_{ob}, min	λ_z, km	Reference
Culgoora	30.3°S	29.2°S	72	244	57	–	*Armstrong* [1982]
Alcantara	2.3°S	0.4°S	48	24	10	17	*Taylor et al.* [1997]
			(15)	(8)	(6)	(9)	
Maui	20.8°N	21.5°N	47	22	10	–	*Taylor et al.* [1995a]
			(17)	(10)	(7)	–	
			53	18	6	17	*Taylor et al.* [1995b]
			(11)	(7)	(4)	(13)	
			52	22	–	7–80	*Isler et al.* [1997]
			(16)	(9)	–	–	
Sacramento Peak	32.8°N	41.5°N	28	23	14	–	*Taylor et al.* [1991]
Nederland	40.0°N	49.0°N	24	35	32	–	*Taylor et al.* [1995d]
			(9)	(14)	(27)	–	
Millstone Hill	42.6°N	53.0°N	47	21	9	17	this study
			(20)	(7)	(5)	(4)	
Pic du Midi	42.9°N	37.8°N	5,17	30,70	–	–	*Moreels and Herse* [1977]
Cime de lat Bonette	44.3°N	39.0°N	15	45	–	–	
Gornergrat	46.0°N	40.9°N	38	26	11	15	*Taylor et al.* [1987]
Sondakyla	67.4°N	63.7°N	16	45	–	–	*Clairemidi et al.* [1985]
Mean values			33	32	12	18	
			(17)	(15)	(8)	(6)	

The computed (or published) mean values of several deduced parameters are listed together with the associated standard deviations in parentheses. In the case of only one or two parameter values, the computed range of values is given. The Culgoora results were not used in deriving the final mean values (see text).

a stable auroral red (SAR) arc. SAR arcs occur commonly at Millstone Hill [*Mendillo et al.* 1989; *Foster et al.*, 1994]. Plates 1c and 1d are 557.7-nm images showing two of the three gravity wave events that occurred on this night; their direction of motion was toward the northwest.

On October 15, the subauroral thermosphere was clearly influenced by geomagnetic activity, but the subauroral mesosphere was not affected in any obvious way. It is possible that the absence of southward wave activity on this night is because any aurorally generated waves were filtered out by equatorward winds. Equatorward neutral wind flow has been shown to occur in the thermosphere during auroral activity [*Foster et al.*, 1994]. While this indeed occurred on October 15, the winds in the mesosphere were small and poleward (<10 m s^{-1}) (D.P. Sipler, private communication, 2000).

8. Discussion

Table 3 lists several previous mesospheric gravity wave results, together with the averages of the deduced c_{ob}, λ_h, τ_{ob}, and λ_z values, and their standard deviations (in parentheses). These studies are listed in order of increasing latitude as a way to place the current set in context. The measured and deduced wave parameters obtained from Millstone Hill were very similar to those obtained from previous gravity wave imaging studies.

For example, at an equatorial site (Alcantara, Brazil [*Taylor et al.*, 1997]) the mean speeds were 48±15 m s^{-1} compared with 47±20 m s^{-1} at Millstone Hill. The mean horizontal wavelengths were 24±8 km compared with 21±7 km at Millstone Hill. *Taylor et al.* [1997] also reported an anisotropic distribution of wave propagation directions. The differences in the directions of the anisotropies between their study and ours at Millstone Hill can be explained by the directions of the originating wave sources relative to each site. The measured horizontal wavelengths and speeds observed at Millstone Hill are also consistent with those reported from the high-latitude study at Sondakyla (67.4°N) [*Clairemidi et al.*, 1985]. The wave event reported by *Armstrong* [1982] was atypical in that the observed wave parameters were significantly larger than those of the other imaging studies. It was therefore not used in the determination of the final mean parameters values in Table 3. A non imaging photometric study of gravity waves in the southern auroral zone (not shown in Table 3) was made by *de Deuge et al.*, [1994]. They reported waves with periods of between 5 to 240 min and speeds of 0 to 300 m s^{-1}. The horizontal wavelengths ranged from 35 to 2000 km, which is much larger than seen in this present study.

Millstone Hill has been an important subauroral site for many years [*Foster et al.*, 1994], being situated at a higher geomagnetic latitude than other midlatitude sites, such as Nederland, Colorado (Table 3), and Bear Lake, Utah. To the authors' knowledge, this study discusses one of the highest geomagnetic latitude data sets in the literature. Our results indicate that while the thermosphere above Millstone Hill is affected often by auroral processes, the occurrence of mesospheric gravity waves seems unrelated to changing levels of geomagnetic activity. Hence the role of auroral processes as a source of the observed mesospheric gravity waves during such periods is apparently minor, as is the case at low latitudes.

9. Summary

Short-period gravity waves have been imaged for the first time at Millstone Hill using a new generation all-sky CCD imaging system. Millstone Hill is in the transition zone between high and middle geomagnetic latitudes. The wave parameters c_{ob}, λ_h, and τ_{ob} were measured from the all-sky images, and the intrinsic wave parameters c_{in}, τ_{in}, and λ_z were deduced using available meteor radar winds. The momentum and energy fluxes of two case study events were also determined. These values were found to be very similar to those reported in other gravity wave imaging studies, implying that the location, and its soon to be upgraded instrumentation, is well suited for such work.

The waves observed in both the pilot and follow-up studies showed a tendency for northward or eastward motion. Millstone Hill lies ~50 km to the west of the Atlantic ocean but no ocean influence was evident in the distribution of the wave directions. Although Millstone Hill is a subauroral site, the data used in this study did not contain a substantial population of gravity waves originating from the auroral zone. Furthermore, there was no clear evidence of an increased frequency of wave events with an equatorward propagation component during geomagnetically active nights (Kp>3). Longer-term studies, especially during highly active geomagnetic periods in the upcoming solar maximum years, will be needed for a more comprehensive investigation of such effects on the frequency and characteristics of IGWs at midlatitudes, particularly in the context of their relationship to the mesospheric mean winds and tides. In addition, optical tomographic reconstruction of gravity waves in height and latitude [see, e.g., *Nygren et al.*, 1998] of some of the events studied here is currently underway using data obtained from the Boston University's COTIF chain of spectrographs [*Semeter and Mendillo*, 1997; *Semeter et al.*, 1999].

Acknowledgments. This work was supported, in part, by a grant from the NSF Aeronomy program and by seed research funds from the Center for Space Physics at Boston University. The authors are grateful to D.P. Sipler for providing additional wind measurements and to Millstone Hill Observatory for continued support for the authors' activities there. The authors would also like to thank the reviewers of this manuscript for their very helpful comments and suggestions. Janet G. Luhmann thanks David C. Fritts, Robert Vincent, and other referees for their assistance in evaluating this paper.

References

Armstrong, E.B., The association of visible airglow features with a gravity wave, *J. Atmos. Terr. Phys., 44*, 325–366, 1982.

Baker, D.J., and A.T. Stair, Rocket measurements of the altitude distributions of the hydroxyl airglow, *Phys. Scr., 37*, 611–622, 1988.

Baumgardner, J., B. Flynn, and M. Mendillo, Monochromatic imaging instrumentation for applications in aeronomy of the Earth and planets, *Opt. Eng., 32*(12), 3028–3032, 1993.

Beer, T., Atmospheric waves and the equatorial ionosphere, *J. Atmos. Terr. Phys., 39*, 971–979, 1977.

Biondi, M.A., D.W. Sipler, M.E. Zipf, and J. Baumgardner, All-sky Doppler interferometer for thermospheric dynamics studies, *Appl. Opt., 33*(10), 1646–1654, 1995.

Booker, J.R., and F.B. Bretherton, The critical layer for internal gravity waves in a shear flow, *J. Fluid Mech., 27*(3), 513–539, 1967.

Clairemidi, J., M. Herse, and G. Moreels, Bi-dimensional observations of waves near the mesopause at auroral latitudes, *Planet. Space Sci., 33*, 1013–1022, 1985.

Clark, R.R., Meteor wind data for global comparisons, *J. Atmos. Terr. Phys., 40*, 905–911, 1978.

Clark, R.R., Upper atmosphere wind observations of waves and tides with the UNH Meteor Radar System at Durham 43°N (1977, 1978 and 1979), *J. Atmos. Terr. Phys., 45*, 621–627, 1983.

Clark, R.R., and J.E. Salah, Propagation of the solar semidiurnal tide in the mesosphere and lower thermosphere at midlatitudes, *J. Geophys. Res., 96*, 1129–1133, 1991.

de Deuge, M.A., P. A. Greet and F. Jacka, Optical observations of gravity waves in the auroral zone, *J. Atmos. Terr. Phys., 56*, 617-629, 1994.

Dewan, E.M., R.H. Picard, R.R. O'Neil, H.A. Gardiner, J. Gibson, J.D. Mill, E. Richards, M. Kendra, and W.O. Gallery, MSX satellite observations of thunderstorm-generated gravity waves in mid-wave infrared images of the upper stratosphere, *Geophys. Res. Lett., 25*(7), 939–942, 1998.

Foster, J.C., M.J. Buonsanto, M. Mendillo, D. Nottingham, F.J. Rich, and W. Denig, Coordinated stable auroral red arc observations: Relationship to plasma convection, *J. Geophys. Res., 99*, 11,429–11,439, 1994.

Francis, S.H., Global propagation of atmospheric gravity waves: A review, *J. Atmos. Terr. Phys., 37*, 1011–1054, 1975.

Freund, J.T., and F. Jacka, Structure in the λ557.7nm [OI] airglow, *J. Atmos. Terr. Phys., 41*, 25–31, 1979.

Fritts, D.C., Gravity wave saturation in the middle atmosphere: A review of theory and observations, *Rev. Geophys., 22*(3), 275–308, 1984.

Galushko, V.G., V.V. Paznukhov, Y.M. Yampolski, and J.C. Foster, Incoherent scatter radar observations of AGW/TID events generated by the moving solar terminator, *Ann. Geophys., 16*, 821–827, 1998.

Garcia, R.R. and S. Solomon, The effect of breaking gravity waves on the dynamics and chemical composition of the mesosphere and lower thermosphere, *J. Geophys. Res., 90*, 3850–3868, 1985.

Gardner, C.S., M. Coble, G.C. Papen, G.R. Swenson, and D.G. Voelz, Observations of the unambiguous 2-dimensional horizontal wave number spectrum of OH intensity perturbations, *Geophys. Res. Lett., 23*(25), 3739–3742, 1996.

Garilov, N.M., and G.M. Shved, Study of internal gravity waves in the lower thermosphere from observations of the nocturnal sky airglow [OI] 5577 Å in Ashkhabad, *Ann. Geophys., 38*, 789–803, 1982.

Greer, R.G.H., and G.T. Best, A rocket-borne photometric investigation of the oxygen lines at 5577 Å and 6300 Å, the sodium D-lines and the continuum at 5300 Å in the night airglow, *Planet. Space Sci., 15*, 1857–1881, 1967.

Hecht, J.H., R.L. Walterscheid, and M.N. Ross, First measurements of the two-dimensional horizontal wave number spectrum from CCD images of the nightglow, *J. Geophys. Res., 99*, 11,449–11,460, 1994.

Hedin, A.E., Extension of the MSIS thermosphere model into the middle and lower atmosphere, *J. Geophys. Res., 96*, 1159–1172, 1991.

Hines, C.O., Momentum deposition by atmospheric waves and its effects on thermospheric circulation, *Space Res., 12*, 1157–1161, 1972.

Hunsucker, R.D., Atmospheric gravity waves generated in the high-latitude ionosphere: A review, *Rev. Geophys., 20*, 293–315, 1982.

Isler, J.R., M.J. Taylor, and D.C. Fritts, Observational evidence of wave ducting and evanescence in the mesosphere, *J. Geophys. Res., 102*, 26,301–26,313. 1997.

Krassovsky, V.I., B.P. Potapov, A.I. Semenov, M.V. Shagaev, N.N. Shefov, V.G. Sobolev and T.I. Toroshelidze, Internal gravity waves near the mesopause and the hydroxyl emission, *Ann. Geophys., 33*, 347–355, 1977.

McLandress, C., On the importance of gravity waves in the middle atmosphere and their parameterization in general circulation models, *J. Atmos. Sol. Terr. Phys., 60*, 1357–1383, 1998.

Mendillo, M., J. Baumgardner, and J. Providakes, Ground-based imaging of detailed arcs, ripples in the diffuse aurora, and patches of 6300-Å emission, *J. Geophys. Res., 94*, 5367–5381, 1989.

Meyer, W., R. Siebenmorgen, and W.-U. Widdel, Estimates of gravity wave momentum fluxes in the winter and summer high mesosphere over northern Scandinavia, *J. Atmos. Terr. Phys., 51*, 311-319, 1989.

Moreels, G., and M. Herse, Photographic evidence of waves around the 85 km level, *Planet. Space Sci., 25*, 265–273, 1977.

Newman, A.L., Nighttime Na D emission observed from a polar-orbiting DMSP satellite, *J. Geophys. Res., 93*, 4067–4075, 1988.

Nygren, T., M.J. Taylor, M.S. Lehtinen, and M. Markkanen, Application of tomographic inversion in studying airglow in the mesopause region, *Ann. Geophys., 16*, 1180–1189, 1998.

Peterson, A.M., Airglow events visible to the naked eye, *Appl. Opt., 18*, 3390–3393, 1979.

Peterson, A.M., and L.M. Kieffaber, Infrared photography of OH airglow structures, *Nature, 242*, 321–322, 1973.

Peterson, A.M., and L.M. Kieffaber, Photography and photometry of the near infrared OH airglow, *Nature, 257*, 649–650, 1975.

Reid, I.M., and R.A. Vincent, Measurements of mesospheric gravity wave momentum fluxes and mean flow accelerations at Adelaide, Australia, *J. Atmos. Terr. Phys., 49*, 443–460, 1987.

Röttger, J., Travelling disturbances in the equatorial ionosphere and their association with penetrative cumulus convection, *J. Atmos. Terr. Phys., 39*, 987–998, 1977.

Semeter, J., and M. Mendillo, A Nonlinear optimization technique for ground-based atmospheric emission tomography, *IEEE Trans., 35*(5), 1105–1116, 1997.

Semeter, J., M. Mendillo, and J. Baumgardner, Multispectral tomographic imaging of the midlatitude aurora, *J. Geophys. Res., 104*, 24,565–24,586, 1999.

Sipler, D.P., J.W. Meriwether and J.E. Salah, Mesospheric

temperature and density over Millstone Hill, *Eos. Trans. AGU 80*(17), Spring Meet. Suppl., S229, 1999

Swenson, G.R., and P.J. Espy, Observations of 2-dimensional airglow structure and Na density from the ALOHA, October 9, 1993 'storm flight', *Geophys. Res. Lett., 22*(20), 2845–2848, 1995.

Swenson, G.R., and C.S. Gardner, Analytical models for the responses of the mesospheric OH^* and Na layers to atmospheric gravity waves, *J. Geophys. Res., 103*, 6271–6294, 1998.

Swenson, G.R., and A.Z. Liu, A model for calculating acoustic gravity wave momentum flux in the mesosphere from OH airglow, *Geophys. Res. Lett., 25*(4), 477–480, 1998.

Swenson, G.R., M.J. Taylor, P.J. Espy, C. Gardner, and X. Tac, ALOHA-93 measurements of intrinsic AGW characteristics using airborne airglow imager and groundbased Na wind/temperature lidar, *Geophys. Res. Lett., 22*(20), 2841–2844, 1995.

Swenson, G.R., R. Haque, W. Yang, and C.S. Gardner, Momentum and energy fluxes of monochromatic gravity waves observed by an OH imager at Starfire Optical Range, New Mexico, *J. Geophys. Res., 104*, 6067–6080, 1999.

Taylor, M.J., and M.A. Hapgood, Identification of a thunderstorm as a source of short period gravity waves in the upper atmospheric nightglow emissions, *Planet. Space Sci., 36*, 975–985, 1988.

Taylor, M.J., and M.A. Hapgood, On the origin of ripple-type wave structure in the OH nightglow emission, *Planet. Space Sci., 38*, 1421–1430, 1990.

Taylor, M.J., and M.J. Hill, Near infrared imaging of hydroxyl wave structure over an ocean site at low latitudes, *Geophys. Res. Lett., 18*(7), 1333-1336, 1991.

Taylor, M.J., M.A. Hapgood, and P. Rothwell, Observations of gravity wave propagation in the OI (557.7 nm), Na (589.2 nm) and the near infrared OH nightglow emissions, *Planet. Space Sci., 35*, 413–427, 1987.

Taylor, M.J., P.J. Espy, D.J. Baker, R.J. Sica, P.C. Neal, and W.R. Pendleton Jr., Simultaneous intensity, temperature and imaging measurements of short period wave structure in the OH nightglow emission, *Planet. Space Sci., 39*, 1171–1188, 1991.

Taylor, M.J., E.H. Ryan, T.F. Tuan and R. Edwards, Evidence of preferential directions for gravity wave propagation due to wind filtering in the middle atmosphere, *J. Geophys. Res., 98*, 6047–6057, 1993.

Taylor, M.J., M.B. Bishop,and V. Taylor, All-sky measurements of short period waves imaged in the OI(557.7 nm), Na(589.2 nm) and near infrared OH and O_2(0,1) nightglow emissions during the ALOHA-93 campaign, *Geophys. Res. Lett., 22*(20), 2833–2836, 1995a.

Taylor, M.J., Y.Y. Gu, X. Tao, C.S. Gardner,and M.B. Bishop, An investigation of intrinsic gravity wave signatures using coordinated lidar and nightglow image measurements, *Geophys. Res. Lett., 22*(20), 2853–2856, 1995b.

Taylor, M.J., D.C. Fritts,and J.R. Isler, Determination of horizontal and vertical structure of an unusual pattern of short period gravity waves imaged during ALOHA-93, *Geophys. Res. Lett., 22*(20), 2837–2840, 1995c.

Taylor, M.J., V. Taylor, and R. Edwards, An investigation of thunderstorms as a source of short period mesospheric gravity waves in *The Upper Mesosphere and Lower Thermosphere: A Review of Experiment and Theory, Geophys. Monogr. Ser.* vol. 87, edited by R.M. Johnson and T.L. Kileen, pp. 177–184, AGU, Washington, D.C.,1995d.

Taylor, M.J., W.R. Pendleton Jr., S. Clark, H. Takahashi, D. Gobbi, and R.A. Goldberg, Image measurements of short-period gravity waves at equatorial latitudes, *J. Geophys. Res., 102*, 26,283–26,299, 1997.

Thomas, R.J., and R.A. Young, Measurements of atomic oxygen and related airglows in the lower thermosphere, *J. Geophys. Res., 85*, 7861–7870, 1980.

Vincent, R.A., Gravity-wave motions in the mesosphere, *J. Atmos. Terr. Phys., 46*, 119–128, 1984.

Walterscheid, R.L., J.H. Hecht, R.A. Vincent, I.M. Reid, J. Woithe, and M.P. Hickey, Analysis and interpretation of airglow and radar observations of quasi-monochromatic gravity wave in the upper mesosphere and lower thermosphere over Adelaide (35°S, 138°E), *J. Terr. and Sol. Atmos. Phys., 61*, 461–478, 1999.

Wang, D.Y., S.P. Zhang, R.H. Wiens, and G.G. Shepherd, Gravity waves from O_2 nightglow during the AIDA'89 campaign III: Effects of gravity wave saturation, *J. Atmos. Terr. Phys., 55*, 397–408, 1993.

Ward, W.E., E.J. Llewellyn, Y. Rochon, C.C. Tai, W.S.C. Brooks, B.H. Solheim, and G.G. Shepherd, Spatial variability in $O(^1S)$ and $O_2(b^1\Sigma^+{}_g)$ emissions as observed with the Wind Imaging Interferometer (WINDII) on UARS in *The Upper Mesosphere and Lower Thermosphere: A Review of Experiment and Theory, Geophys. Monogr. Ser.* vol. 87, edited by R.M. Johnson and T.L. Kileen, pp. 323–328, AGU, Washington, D.C.,1995.

J. Baumgardner, M. Mendillo, and S.M. Smith, Center for Space Physics, Boston University, 725 Commonwealth Ave., Boston, MA 02215. (e-mail: jeff@spica.bu.edu; mendillo@bu.edu; smsm@bu.edu)

R.R. Clark, Department of Electrical and Computer Engineering, University of New Hampshire, Durham, NH 03824. (e-mail: ron.clark@unh.edu)

(Received April 23, 1999; revised March 8, 2000; accepted April 3, 2000.)